Inorg. Chem. **2006**, *45*, 1184–1191

Coupled Ion/Electron Hopping in Li_xNiO_2: A ^7Li NMR Study

C. Chazel, M. Ménétrier,* L. Croguennec, and C. Delmas

Institut de Chimie de la Matière Condensée de Bordeaux−CNRS and ENSCPB, Université Bordeaux 1, 87 Av. Schweitzer, 33608 PESSAC Cedex, France

Received September 16, 2005

Deintercalated "Li_xNiO_2" materials ($x = 0.25$, 0.33, 0.50, 0.58, and 0.65) were obtained using the electrochemical route from the $Li_{0.985}Ni_{1.015}O_2$ and $Li_{0.993}Ni_{1.007}O_2$ compounds. Refinements of X-ray diffraction data using the Rietveld method show a good agreement with the phase diagram of the Li_xNiO_2 system studied earlier in this laboratory. Electronic conductivity measurements show a thermally activated electron-hopping process for the deintercalated $Li_{0.5}NiO_2$ phase. In the Li_xNiO_2 materials investigated ($x = 0.25$, 0.33, 0.50, and 0.58), ^7Li NMR shows mobility effects leading to an exchanged signal at room temperature. A clear tendency for Li to be surrounded mainly by Ni^{3+} ions with the 180° configuration is observed, particularly, for strongly deintercalated materials with smaller Li^+ and Ni^{3+} contents, even upon heating, when this mobility becomes very fast in the NMR time scale. This suggests that Li/vacancy hopping does occur on the NMR time scale but that Ni^{3+}/Ni^{4+} hopping does not occur independently. The position of Li seems to govern the oxidation state of the Ni around it at any time; the electrons follow the Li ions to satisfy local electroneutrality and minimal energy configuration. The observed NMR shifts are compatible with the Li/vacancy and Ni^{3+}/Ni^{4+} ordering patterns calculated by Arroyo y de Dompablo et al. for $x = 0.25$ and $x = 0.50$, but not for $x = 0.33$ and $x = 0.58$.

Introduction

Li NMR measurements of transition metal oxides, such as the positive electrodes for Li-ion batteries, are very specific insofar as the electron spins carried by metal ions induce characteristic (so-called hyperfine) interactions on the Li nucleus: the dipolar and Fermi-contact (or Knight) interactions (ref 1 and references therein). As a result ^7Li NMR is a good probe to study the local Li environment in terms of transition metal cations and their oxidation state. Several studies have reported the Ni^{3+} ($t_{2g}^6\ e_g^1$) effect on the ^7Li NMR spectra for $LiNi_{0.30}Co_{0.70}O_2$ and deintercalated phases.[2,3] In the starting material, NMR allowed the different Li environments to be distinguished depending on the number and position of Ni^{3+} ions around Li: 90° (edge-sharing) and 180° (corner-sharing) Li−O−Ni^{3+} interactions. A ^7Li NMR study of the corresponding deintercalated materials showed that Ni^{3+} oxidation into diamagnetic Ni^{4+} occurred first, leading to an exchanged NMR signal from the independent ionic and electronic hopping, whose position continuously shifts to 0 ppm: Li feels an average number of Ni ions (ionic hopping) with an average Ni oxidation state (electronic hopping).[3]

In addition, the Li_xNiO_2 system has been extensively studied over the past years because of its application as a positive electrode material for lithium-ion batteries.[4−7] Its electrochemical properties are mainly characterized by a high reversible capacity, and the electrochemical curve, $V = f(x)$, exhibits a large number of plateaus, which highlight the structural modifications that occur upon Li deintercalation. The latter have been characterized in detail by the Ohzuku,[5] Dahn,[6] and Kanno[7] research groups and by our lab;[8−10] a monoclinic lattice in a large composition range, between about $x = 0.75$ and $x = 0.50$, has been shown for the Li_x-

* To whom correspondence should be addressed. Phone: +33 5 40 00 66 39. Fax: +33 5 40 00 27 61. E-mail: menetrier@icmcb-bordeaux.cnrs.fr.

(1) Grey, C. P.; Dupre, N. *Chem. Rev.* **2004**, *104*, 4493.
(2) Marichal, C.; Hirschinger, J.; Granger, P.; Ménétrier, M.; Rougier, A.; Delmas, C. *Inorg. Chem.* **1995**, *34*, 1773.
(3) Carlier, D.; Ménétrier, M.; Delmas, C. *J. Mater. Chem.* **2001**, *11*, 594.
(4) Goodenough, J. B.; Wickham, D. G.; Croft, W. J. *J. Phys. Chem. Solids* **1958**, *5*, 107.
(5) Ohzuku, T.; Ueda, A.; Nagayama, M. *J. Electrochem. Soc.* **1993**, *140*, 1862.
(6) Li, W.; Reimers, J. N.; Dahn, J. R. *Solid State Ionics* **1993**, *67*, 123.
(7) Hirano, A.; Kanno, R.; Kawamoto, Y.; Takeda, Y.; Yamaura, K.; Takano, M.; Ohyama, K.; Ohashi, M.; Yamaguchi, Y. *Solid State Ionics* **1995**, *78*, 123.
(8) Pérès, J. P.; Delmas, C.; Rougier, A.; Broussely, M.; Perton, F.; Biensan, P.; Willmann, P. *J. Phys. Chem. Solids* **1996**, *57*, 1057.
(9) Pérès, J. P.; Demourgues, A.; Delmas, C. *Solid State Ionics* **1998**, *111*, 135.
(10) Pérès, J. P.; Weill, F.; Delmas, C. *Solid State Ionics* **1999**, *116*, 19.

10.1021/ic051593n CCC: $33.50
Published on Web 01/07/2006

NiO_2 system. Nevertheless, the lower limit of the monoclinic distortion was found to be slightly different by Arai et al. ($x = 0.38$)[11] and our lab ($x = 0.40$).[8,12] Ohzuku et al. have suggested that this structural modification was related to a cooperative distortion of NiO_6 octahedra resulting from the Jahn−Teller effect of trivalent nickel ions in the low-spin state $t_{2g}^6e_g^1$ as was previously reported for $NaNiO_2$.[13] However an EXAFS study for the monoclinic $Li_{0.63}Ni_{1.02}O_2$ phase[9] has shown that the average distortion of the NiO_6 octahedra was considerably reduced compared with that of $LiNiO_2$ itself, which is not macroscopically distorted according to XRD;[14] as a result, the Jahn−Teller effect could not explain the monoclinic transition. A selected area electron diffraction study carried out by Pérès et al.[10] on the $Li_{0.63}Ni_{1.02}O_2$ material showed that the structure of this phase involves a doubling of the *a* and *b* parameters from those deduced by X-ray diffraction experiments and suggested that the origin of the superstructure could be explained by Li/vacancy orderings during the charge of the Li//Li_xNiO_2 battery. Superstructures were also shown by electron diffraction for the $x = 0.25$ and $x = 0.33$ compositions.[15]

Theoretical studies have also been carried out on the Li_xNiO_2 system. Arroyo y de Dompablo et al. used first-principles DFT calculations (pseudopotential method with the generalized gradient approximation) that yielded detailed information about relative stability and local structure as a function of composition to clarify the phase diagram of Li_xNiO_2.[16] They proposed Li/vacancy ordering schemes, coupled with a Ni^{3+}/Ni^{4+} ordering for some particular compositions: $x = 1/4$, 1/3, 2/5, 1/2, 3/5, and 3/4[16] and $x = 2/3$[17] and suggested that the driving force to obtain such orderings was the presence of 180° Li−O−Ni^{3+}−O−Li interactions that stabilize the Jahn−Teller environment around Ni^{3+} ions and thus the structure. $^{6/7}$Li NMR experiments were reported for the pristine $LiNiO_2$ material, and the isotropic position was first found to be at 580 ppm by Ganguly et al.[18] and at 726 ppm by Carlier et al. using ^{7}Li NMR at 77.7 MHz[19] and by Chazel et al. using $^{6/7}$Li NMR experiments at 44 and 116 MHz.[20]

On the basis of these recent results we used ^{7}Li NMR to investigate the Li interactions with paramagnetic Ni^{3+} ions ($t_{2g}^6e_g^1$) upon oxidation into Ni^{4+} in the context of possible Li/vacancy and Ni^{3+}/Ni^{4+} orderings and to show the effect of ionic and electronic hopping on the NMR spectra.

Experimental Section

The starting materials $Li_{1-z}Ni_{1+z}O_2$ were obtained by the coprecipitation route described elsewhere.[20] Refinement of XRD data using the Rietveld method showed that $z = 0.015(4)$ and $z = 0.007(5)$ for the samples used in batteries as follows. The pristine materials were therefore referred to as quasi-stoichiometric $LiNiO_2$ and the corresponding deintercalated phases as Li_xNiO_2 in the following (except in the magnetism results section where the accurate stoichiometry will be given for each material).

The Li_xNiO_2 phases ($x = 0.25$, 0.33, 0.58, and 0.65) were obtained by electrochemical deintercalation of the $Li_{0.985}Ni_{1.015}O_2$ phase using Li/$LiPF_6$, PC, EC, DMC/$Li_{0.985}Ni_{1.015}O_2$ cells. The positive electrode consisted of a $LiNiO_2$/carbon/graphite (1/1) (90−10 wt %) mixture. For $Li_{0.50}NiO_2$, the electrode consisted of a pressed pellet (8 mm in diameter, 800 MPa in compression) of pure $Li_{0.993}Ni_{1.007}O_2$. The cells were charged at room temperature with a C/300 (C/200 for $Li_{0.5}NiO_2$) rate and alternate periods of relaxation. The voltage stability criterion for the relaxation periods was fixed at 1 mV/h. The positive electrodes were recovered at the target value, x_{elec}, after being relaxed, washed with DMC, and vacuum dried in an argon-filled glovebox. For each battery, the final open circuit voltage was measured after a very long relaxation time and was found to be consistent with that from the electrochemical cycling curve of $LiNiO_2$ established previously in our lab.[10,12]

X-ray diffraction patterns of the different lithium nickelates synthesized were recorded using a Siemens D5000 powder diffractometer with Cu Kα radiation and a graphite-diffracted beam monochromator. For structural study by the Rietveld method, data were collected in the 5−120° (2θ) range in steps of 0.02° (2θ) with a constant counting time of 40 s. Refinement of the X-ray diffraction data was achieved using the full-pattern matching method (FULLPROF program[21]). Since the deintercalated phases are hygroscopic, the XRD samples were prepared in an argon-filled glovebox using airtight sample holders.

Magnetic measurements were recorded using a SQUID (superconducting quantum interference device) MPMS-5S. For three samples ($x = 0.33$, 0.58, and 0.65), the magnetization, *M*, was investigated as a function of the applied field, *H* (-2000 Oe $< H < 2000$ Oe), at 5 K and as a function of temperature, *T* (5 K $< T <$ 300 K), at two given fields ($H = 500$ and 10 000 Oe) (zero-field-cooled susceptibility).

The electronic conductivity measurements were carried out on (unsintered) pellets recovered from the electrochemical cell after partial Li deintercalation using the four-probe method with direct current in the 140−400 K range.

^{7}Li MAS NMR spectra were recorded on a Bruker 300 Avance spectrometer at 116 MHz (7.05 T magnet) with a standard 4 mm Bruker MAS probe. The samples were mixed with dry silica to facilitate spinning and to improve the field homogeneity, since they may exhibit metallic or paramagnetic properties. The mixture was placed into a 4 mm diameter zirconia rotor in the drybox. A combination of single pulse and Hahn echo sequences was used in MAS conditions (10 kHz and 15 kHz spinning speeds) for all phases. The single pulse sequence with $t_\pi/2 = 2.4$ μs requires a first-order phasing process with a sin *x*/*x* baseline correction because

(11) Arai, H.; Okada, S.; Ohtsuka, H.; Ichimura, M.; Yamaki, J. *Solid State Ionics* **1995**, *80*, 261.
(12) Croguennec, L.; Pouillerie, C.; Delmas, C. *J. Electrochem. Soc.* **2000**, *147*, 1314.
(13) Dyer, L. D.; Borie, B. S., Jr.; Smith, G. P. *J. Am. Chem. Soc.* **1954**, *76*, 1499.
(14) Rougier, A.; Delmas, C.; Chadwick, A. V. *Solid State Commun.* **1995**, *94*, 123.
(15) Delmas, C.; Ménétrier, M.; Croguennec, L.; Levasseur, S.; Pérès, J. P.; Pouillerie, C.; Prado, G.; Fournès, L.; Weill, F. *Int. J. Inorg. Mater.* **1999**, *1*, 11.
(16) Arroyo y de Dompablo, M. E.; Van der Ven, A.; Ceder, G. *Phys. Rev. B* **2002**, *66*, 64112.
(17) Arroyo y de Dompablo, M. E.; Marianetti, C.; Van der Ven, A.; Ceder, G. *Phys. Rev. B* **2001**, *63*, 144107.
(18) Ganguly, P.; Ramaswamy, V.; Mulla, I. S.; Shinde, R. F.; Bakare, P. P.; Ganapathy, S.; Rajamohanan, P. R.; Prakash, N. V. K. *Phys. Rev. B* **1992**, *46*, 11595.
(19) Carlier, D.; Ménétrier, M.; Grey, C. P.; Delmas, C.; Ceder, G. *Phys. Rev. B* **2003**, *67*, 174103 1.
(20) Chazel, C.; Ménétrier, M.; Croguennec, L.; Delmas, C. *Magn. Reson. Chem.* **2005**, *43*, 849.
(21) Rodriguez-Carvajal, J. Laboratoire Léon Brillouin, http://www-llb.cea.fr/fullweb/powder.htm, 2004.

Table 1. Results Obtained from the Refinement of the XRD Data of the Li_xNiO_2 Phases using the Rietveld (R) or Full-Pattern Matching (fpm) Method

		0.25	0.33	0.50	0.58	0.65
phase 1	space group	$R\bar{3}m$	$R\bar{3}m$	$C2/m$	$C2/m$	$C2/m$
	a (Å)	2.8263(5)	2.8243(7)	4.937(1)	4.9667(6)	4.9875(8)
	b (Å)	2.8263(5)	2.8243(7)	2.8293(8)	2.8282(4)	2.8290(4)
	c (Å)	14.402(4)	14.416(5)	5.077(2)	5.0761(8)	5.0615(8)
	β (deg)			109.19(1)	109.535(8)	109.74(1)
	R_{wp}	14.2	14.9	18.5	10.4	12.5
phase 2	space group	$R\bar{3}m$				
	a (Å)	2.819(2)				
	b (Å)	2.819(2)				
	c (Å)	13.432(7)				
	β (deg)					
	R_{wp}	14.2				

of the dead time of the spectrometer. The Hahn echo sequence [$t_\pi/2 - \tau_1 - t_\pi - \tau_2$] was used to facilitate the phasing of all the signals and to ensure the observation of possible very wide signals which are lost during the receiver dead time, while refocusing the interactions with electron spins.[20] The 90° pulse duration was equal to $t_\pi/2 = 2.4\ \mu$s. Variable-temperature (VT) NMR experiments were also carried out on the deintercalated compounds. The temperature indicated is the one measured by a thermocouple and corresponds to that of the gas that heats the rotor. For each temperature, we waited 15 min for temperature equilibrium before carrying out NMR experiments. In an earlier paper using lead nitrate as a temperature indicator, we showed that the friction of the drive gas flow on the rotor causes a temperature increase of 7 K when spinning at 10 kHz and 23 K when spinning at 15 kHz. Although this standardization process was not repeated upon heating, we can assume that the actual temperature in the rotor is higher by these amounts than the one indicated. Note also that the temperature difference induced by the change in spinning speed from 10 to 15 kHz was taken into account when determining the isotropic signal as explained earlier.[20]

Results and Discussion

X-ray Diffraction. Table 1 summarizes the results obtained from the refinements of the X-ray diffraction data for the deintercalated phases. All these data are in agreement with the phase diagram of the Li_xNiO_2 system previously studied in our laboratory.[10,12] Indeed, the refinement of the XRD pattern of $Li_{0.25}NiO_2$ showed the presence of two rhombohedral phases (corresponding to the R2/R3 electrochemical plateau), whereas for $x = 0.33$, 0.50, 0.58, and 0.65, single phases were obtained as expected by the Li_xNiO_2 charge curve,[12] the first phase being rhombohedral and the latter three monoclinic.

The evolution of the lattice parameter, c_{hex}, as a function of x was found to be consistent with the results obtained for the deintercalated $Li_xNi_{1.02}O_2$ phases.[22]

Magnetic Susceptibility Measurements. Figure 1 shows the variation of the magnetization, M, of three deintercalated phases ($x = 0.33$, 0.58, and 0.65) and of the starting lithium nickelate $Li_{0.985}Ni_{1.015}O_2$ as a function of the applied magnetic field, H. The starting material exhibits a hysteresis loop related to interlayer ferromagnetic interactions, which was already discussed in previous papers.[23−25] For deintercalated

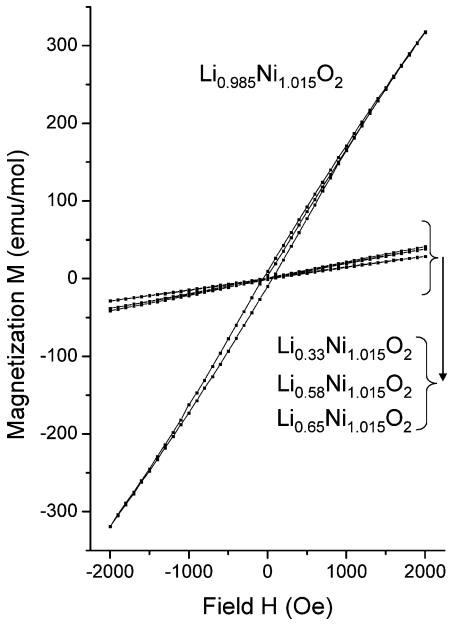

Figure 1. Variation of the magnetization, M, as a function of the applied magnetic field, H, recorded at 5 K for $Li_{0.33}Ni_{1.015}O_2$, $Li_{0.57}Ni_{1.015}O_2$, $Li_{0.67}Ni_{1.015}O_2$, and $Li_{0.985}Ni_{1.015}O_2$.

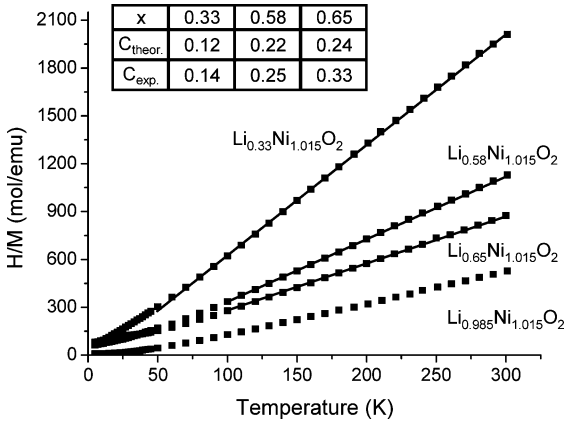

Figure 2. Variation of the reciprocal zero-field-cooled magnetic susceptibility as a function of temperature recorded at 10000 Oe for $Li_{0.33}Ni_{1.015}O_2$, $Li_{0.57}Ni_{1.015}O_2$, $Li_{0.67}Ni_{1.015}O_2$, and $Li_{0.985}Ni_{1.015}O_2$. The theoretical and experimental Curie constants of the deintercalated phases are given. The linear domain $H/M = f(T)$ taken into account in the calculation of the experimental Curie constant is represented by a line for each deintercalated phase.

phases, the hysteresis loop has practically disappeared; the magnetization, M, is in first approximation directly proportional to the applied field, H. We attribute this effect to oxidation of Ni^{2+} to the 3+ state in the Li site and to a mixed Ni^{3+}/Ni^{4+} state in the transition metal layer. This was confirmed by the susceptibility measurements shown in Figure 2 where the variation of the H/M ratio vs temperature obeys the Curie−Weiss law. In the paramagnetic domain, the H/M ratio is equal to the inverse of susceptibility, which is directly proportional to the temperature via the Curie

(22) Croguennec, L.; Pouillerie, C.; Mansour, A. N.; Delmas, C. *J. Mater. Chem.* **2001**, *11*, 131.

(23) Rougier, A.; Delmas, C.; Chouteau, G. *J. Phys. Chem. Solids* **1996**, *57*, 1101.

(24) Barra, A. L.; Chouteau, G.; Stepanov, A.; Delmas, C. *J. Magn. Magn. Mater.* **1998**, *177−181*, 783.

(25) Barra, A. L.; Chouteau, G.; Stepanov, A.; Rougier, A.; Delmas, C. *Eur. Phys. J. B* **1999**, *7*, 551.

constant. We consider that the relatively good agreement observed in Figure 2 between experimental (deduced from the slope of the linear domain) and theoretical (calculated for the above-mentioned oxidation state of Ni ions by taking into account the actual stoichiometry for each material) Curie constants confirms the Ni^{3+}/Ni^{4+} ratio present in each deintercalated phase. Note that such an agreement was not obtained for the pristine $Li_{0.985}Ni_{1.015}O_2$ phase, which confirms the absence of ferrimagnetic clusters in the deintercalated phases.

Electronic Properties. The conductivity of $Li_{0.50}NiO_2$ is thermally activated, which evidences an electronic-hopping process within the material. The thermal variation of the logarithm of conductivity for $Li_{0.50}NiO_2$ does not strictly obey an Arrhenius law (the activation energy E_a slightly varies with temperature: E_a is equal to 0.25 and 0.19 eV in the 295−395 and 180−275 K ranges, respectively). The activation energy is in the normal range observed for small polaron conductivity in oxides. Indeed the experimental value is quite similar to that observed for the deintercalated $Li_{0.72}Ni_{0.30}Co_{0.70}O_2$ ($\Delta E = 0.27$ eV)[3]. In addition, the $Li_{0.50}NiO_2$ phase exhibits an electronic conductivity equal to $10^{-2.3}$ S cm^{-1} at room temperature.

^{7}Li NMR. Preliminary Study. The goal was to use the Li/vacancy and Ni^{3+}/Ni^{4+} ordering patterns shown by Arroyo y de Dompablo et al. for two layers (one lithium and one nickel)[16] to build up the adjacent Ni and Li layers to determine for each composition the number of Ni^{3+} and Ni^{4+} ions surrounding Li (90° and 180° configurations). This construction is necessary to estimate the shift due to Ni^{3+} on the basis of the previous NMR studies carried out on the $LiNi_{0.30}Co_{0.70}O_2$ phase giving the shift due to Ni^{3+} in the 90° and 180° Li−O−Ni^{3+} configurations.[2,3]

Thus, the first step consisted of building several adjacent Ni and Li layers according to Arroyo y de Dompablo's ordering schemes by considering that the 180° Li−O−Ni^{3+}−O−Li configuration was the criterion, as stated by Arroyo y de Dompablo et al., allowing Jahn−Teller distortion of the $Ni^{3+}O_6$ octahedra, for energy minimization of the O3-type Li_xNiO_2 structure. This was carried out for $x = 1/4$, 1/3, 3/5,[16] and 2/3,[17] which are the established patterns closest to our deintercalated samples. Actually, these constructions were not so obvious for the $x = 1/2$, 3/5, and 2/3 compositions since the first-principle calculations predicted the presence of "$Ni^{3.5+}$" ions in the most stable configurations.[16,17] However we decided not to take into account the existence of these $Ni^{3.5+}$ ions that might be an artifact of calculation.[26] As a result, the following step was to find new Ni^{3+}/Ni^{4+} schemes based on the proposed Li/vacancy ordering (180° Li−O−Ni^{3+}−O−Li configuration) that satisfied the criterion of energy minimization. This was achieved for $x = 1/2$ and 3/5 compositions, but no satisfactory pattern could be determined for the $Li_{2/3}NiO_2$ phase.

Once the first adjacent Li and Ni layers (called Li_{lower} and Ni_{lower}) were formed (directly given by Arroyo y de Dompablo's ordering schemes or determined for peculiar com-

(26) Ceder, G. Private Communication.

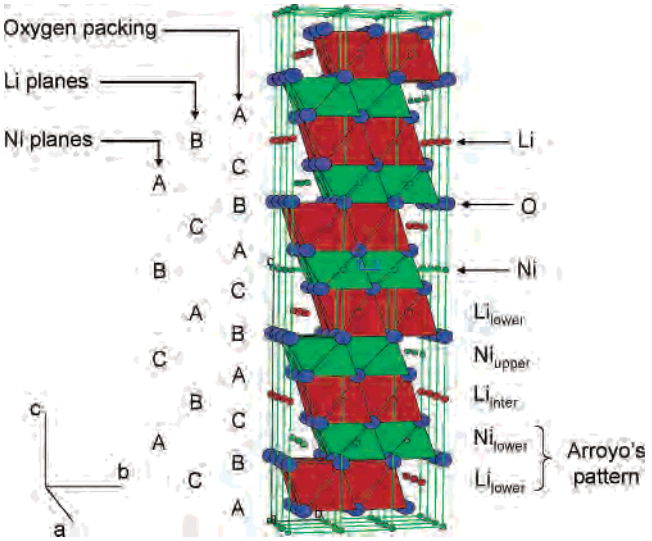

Figure 3. Oxygen, lithium, and nickel packings of the O3-type Li_xNiO_2 structure showing the construction of the next adjacent Li and Ni layers from Arroyo y de Dompablo's patterns.

positions as decribed above), we constructed two other Li layers (the intermediate Li layer called Li_{inter} and the upper one called Li_{upper}) and another Ni layer (the upper Ni layer called Ni_{upper}) as shown in Figure 3. A total of five layers (three Li and 2 Ni layers) are thus necessary to determine the Li environments from the Li_{inter}, Ni_{lower}, and Ni_{upper} layers. This construction has to follow two conditions. The first one, the structural condition, is consideration of the O3-type Li_xNiO_2 structure described by an AB CA BC oxygen packing in the triangular lattice with the three, A, B, C, possible atomic positions. The C and A sites for Li_{lower} and Ni_{lower}, respectively, were chosen arbitrarily to make it easy to deduce the sites occupied by Li and Ni belonging to the next adjacent layers as shown in Figure 3. Then Li_{inter} and Ni_{upper} are located in the B and C sites, whereas Li_{upper} is in the A site. The second condition, the "minimization energy" condition, consists of finding the 180° Li_{lower}−$Ni^{3+}{}_{lower}$−Li_{inter} and 180° Li_{inter}−$Ni^{3+}{}_{upper}$−Li_{upper} interactions that stabilize the structure as stated by Arroyo y de Dompablo. To illustrate this construction, the Li/vacancy ordering, found both by electron diffraction and first-principle calculation, for the $x = 1/3$ composition is taken as an example. The first two Li layers and the first Ni layer are represented in Figure 4 to illustrate the Li^+/Ni^{3+} relative positions. The whole construction is not presented for clarity.

The next step consisted of observing the Ni^{3+}/Ni^{4+} arrangements around Li_{inter} considering the Ni_{lower} and Ni_{upper} layers and distinguishing the two possible Ni^{3+}−O−Li arrangements (90° and 180° Ni−O−Li configuration) to finally estimate the shift in the deintercalated Li_xNiO_2 phases according to previous studies on $LiNi_{0.30}Co_{0.70}O_2$ (i.e., by considering that each Ni^{3+} ion in the 180° configuration causes a +110 ppm shift and each Ni^{3+} ion in the 90° configuration causes a −15 ppm shift).[2,3] The different Li environments and the corresponding shifts are summarized in Table 2. For the $x = 3/5$ composition, two different environments for Li have been determined leading to two different estimated shifts. For the $x = 2/3$ composition, no

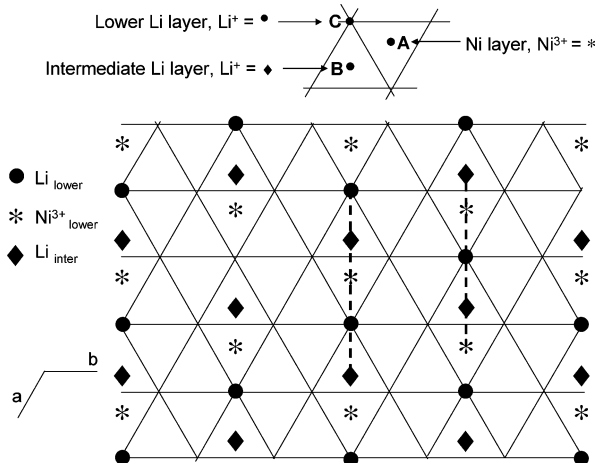

Figure 4. Projection in the (*a*,*b*) plane of the first two Li layers and the first Ni layer. Li^+ atoms in the lower and intermediate layers are respectively represented by ● and ◆, the other positions being vacancies. Ni^{3+} ions in the lower Ni layer are represented by *, the other positions being occupied by Ni^{4+} ions. The 180° Li−O−Ni^{3+}−O−Li interaction responsible for the stabilization of the structure is illustrated by a dashed line. The whole construction (3 Li layers and 2 Ni layers) is not presented for clarity.

Table 2. Number of Ni^{3+} Ions Surrounding Li According to the Construction Described in the Text and the Corresponding Calculated NMR Shifts for Li_xNiO_2 Phases

	no. of Ni^{3+} surrounding Li		estimated shifts
x	90°	180°	(ppm)
1/4	0	6	660
1/3	2	2	190
1/2	2	6	630
3/5	4	2	160 (2/3)
	2	6	630 (1/3)
2/3	?	?	?

shifts were estimated since no satisfactory global pattern could be established.

NMR Results. Figure 5a shows the single pulse ^7Li MAS NMR spectra of the deintercalated phases ($x = 0.25$, 0.33, 0.50, 0.58, and 0.65) recorded at 15 kHz. The significantly lower signal-to-noise ratio observed for $x = 0.33$ is simply the result of the fact that this spectrum was recorded with a number of scans equal to half that used for the other compositions. The single-pulse MAS NMR spectra show a 0 ppm signal for each phase corresponding to the presence of lithium carbonate in the pristine $LiNiO_2$ material as previously shown by XRD and ^7Li NMR[20] and to that of the solid electrolyte interphase.[27] A broad signal, corresponding to Li in the Li_xNiO_2 material, more or less separated into spinning sidebands depending on the composition is also observed at higher ppm values. For each material, the isotropic positions, summarized in Table 3, were determined using the 10 kHz and 15 kHz spinning speeds and compared with the estimated shifts deduced from the Li/vacancy and Ni^{3+}/Ni^{4+} ordering schemes determined as discussed above. It appears that the experimental shift is always lower than that expected from the ordering schemes. Moreover, the striking fact is that the experimental shift increases upon Li deintercalation, whereas the number of paramagnetic Ni^{3+} ions in the material, responsible for the NMR shift, decreases when Li is deintercalated from the positive electrode (oxidation). These observations suggest a nonrandom Ni^{3+}/Ni^{4+} arrangement around Li and also a complex ionic or electronic hopping on the NMR observation time scale, which we will explore in more detail in the following using echo and variable-temperature (VT) NMR experiments.

(27) Ménétrier, M.; Vaysse, C.; Croguennec, L.; Delmas, C.; Jordy, C.; Bonhomme, F.; Biensan, P. *Electrochem. Solid State Lett.* **2004**, *7* (6), A140.

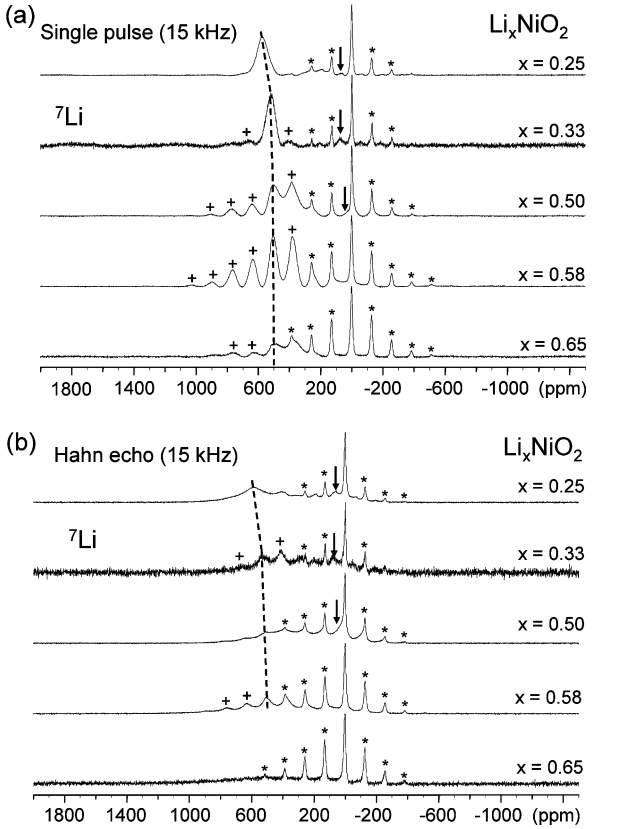

Figure 5. (a) Single-pulse and (b) synchronized-echo ^7Li MAS NMR spectra of the deintercalated Li_xNiO_2 phases ($x = 0.25$, 0.33, 0.50, 0.58, and 0.65) (116.7 MHz, 15 kHz spinning, arbitrary intensities, (* and +) spinning sidebands). Minor signals are represented by an arrow.

Table 3. Comparison between the Experimental, Calculated (Li/vacancy and Ni^{3+}/Ni^{4+} ordering patterns), and the Full-Exchange (averaged $Ni^{(4-x)+}$ oxidation state) Shifts for the Li_xNiO_2 Phases[a]

x	observed shifts (ppm)	estimated shifts (ppm) (ordering patterns)		full-exchange shifts (ppm)
0.25	570 75 (minority)	660		142
0.33	530 80 (minority)	190		188
0.50	510 30 (minority)	630		285
0.58	510	160 (2/3) 630 (1/3)	316	331
0.65	470	?		371

[a] For $x = 0.58$, 316 ppm is the barycenter of the two positions. Minor signals observed in NMR are also mentioned (see text).

Synchronized-echo ^7Li MAS NMR spectra plotted in Figure 5b also show the 0 ppm signal, whereas the broad shifted signal is hardly observed regardless of the composition. The significantly lower signal-to-noise ratio observed for $x = 0.33$ is simply because this spectrum was recorded with a number of scans equal to one-fourth of that used for the other compositions. In the Hahn echo sequence, the

nuclear spins are normally refocused by the second RF pulse, which reverts the dephasing of the individual spins essentially because of interactions with the electron spins of Ni^{3+} in their various environments in the material. If a change in the spin system due to mobility occurs in this period of time, refocusing cannot take place. In a MAS experiment, the interpulse delay is fixed to one rotor period for the second pulse to arise when the sample is in the same position as for the first pulse, which corresponds to 67 μs (refocusing delay) for the 15 kHz spinning speed used. Therefore, the loss of echo signal observation is the result of a movement with a frequency in the 10 kHz order of magnitude, leading to a decrease of the apparent T_2 relaxation time, as would be measured using variable-delay Hahn echo experiments (with an increasing number of rotor periods as the interpulse delay). If the movement is faster, the apparent T_2 relaxation time increases and the echo observation is restored (see the VT experiments in the following). Another effect of mobility for the NMR is the exchange of individual NMR signals when hopping of the probed species between the corresponding environments occurs with a frequency higher than the separation (in Hertz) of the individual signals. In this respect, 10 kHz corresponds to a difference in NMR shifts close to 100 ppm in our conditions, which means that when movements lead to a weak echo observation, any individual signals separated by up to a few hundreds of ppm are also, at least partially, exchanged.

In Table 3, we have therefore also indicated the estimated shift for a "full-exchange" situation, corresponding to a fast Ni^{3+}/Ni^{4+} hopping. This estimation considers that each Ni ion has an average oxidation state $4 - x$ and causes a corresponding portion of the shift due to Ni^{3+} on the neighboring Li ions in each configuration (90° and 180°). Note that Li/vacancy hopping is not required for such a situation, since all Li ions have identical environment in terms of number of Ni ions.

On this basis, we now discuss the results shown in Table 3 and Figure 5, as well as those of the VT MAS NMR measurements carried out in selected cases, for the various materials.

For all the materials, the room-temperature echo signal is weaker than the single-pulse one, which means that mobility in the 10 kHz time scale occurs (Figure 5).

$Li_{0.25}NiO_2$. The observed shift is much higher than the full-exchange one, and somewhat smaller than the calculated one, which considers that each Li ion is surrounded by 6 Ni^{3+} with the 180° configuration.

$Li_{0.33}NiO_2$. The ordering pattern suggests only 2 Ni^{3+} with 180° and 2 Ni^{3+} with 90° configuration around each Li. The experimental shift is incompatible with this pattern and again much higher than in a fully exchanged situation (Table 3). Figure 6 shows the single-pulse and synchronized-echo ^{7}Li MAS NMR spectra of the $Li_{0.33}NiO_2$ phase recorded at variable temperature (295 K < T < 403 K) using a 15 kHz spinning speed. Echo signal observation is recovered at high temperature and the single-pulse line becomes narrower upon heating because of the averaging of the dipolar interaction (motional narrowing), which means that the movement is very fast, and the signal is therefore exchanged at higher temperature. Since no change in the signal other than a broadening and a regular decrease in the Fermi contact shift (which is the result of the decrease in paramagnetic susceptibility[20]) occurs between room temperature and 353 K, we conclude that the room temperature (RT) signal is already exchanged. The NMR signal recorded at 403 K using the Hahn echo sequence is really different from that recorded at 353 K as if the mobility became slow. Indeed the NMR signal corresponding to the material strongly decreases in magnitude for the echo sequence, and the weak NMR signal observed at 80 ppm at room temperature that we assigned to a minor impurity (Table 3) drastically increases in intensity as shown in the synchronized-echo spectrum. As discussed in a forthcoming paper, this is related to the beginning of the transformation of the deintercalated phase at 403 K since $LiNiO_2$ is well-known for being unstable at the charged state, transforming into a spinel phase. Indeed Guilmard et al. showed, using in situ X-ray diffraction, that the latter is usually obtained from the $Li_{0.5}NiO_2$ phase at about 473 K and even at lower temperature for $x < 0.5$[28]. The spectra recorded both in single-pulse and Hahn echo sequences at room temperature after heating to 353 K in the variable-temperature experiment clearly confirm that a structural modification occurred within the material since they are very different from those obtained at room temperature before heating.

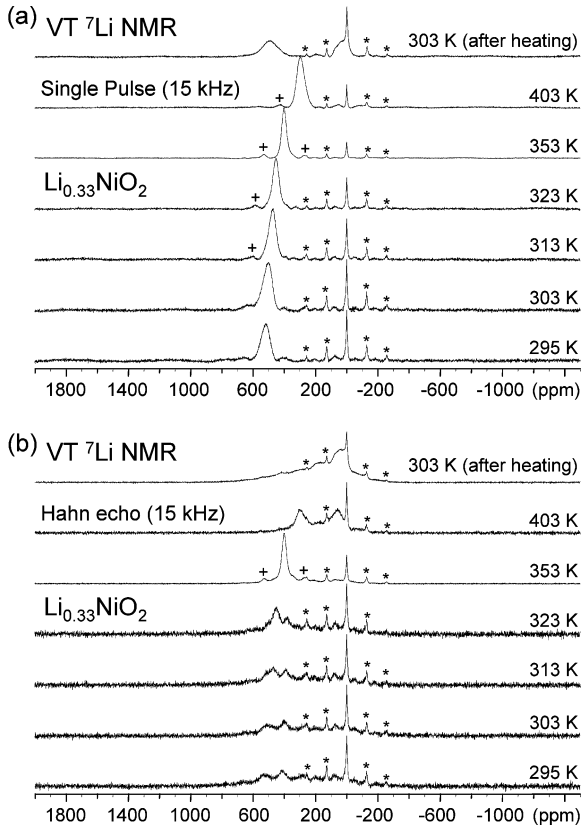

Figure 6. (a) Single-pulse and (b) synchronized-echo ^{7}Li MAS VT NMR spectra of $Li_{0.33}NiO_2$ (116.7 MHz, 15 kHz spinning, arbitrary intensities, (* and +) spinning sidebands, 295 K < T < 403 K).

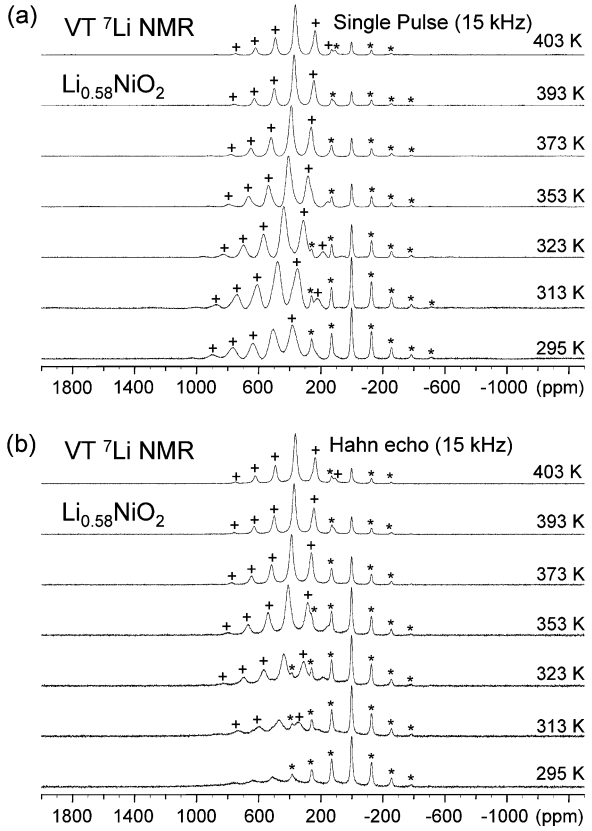

Figure 7. (a) Single-pulse and (b) synchronized-echo ^{7}Li MAS VT NMR spectra of $Li_{0.58}NiO_2$ (116.7 MHz, 15 kHz spinning, arbitrary intensities, (* and +) spinning sidebands, 295 K < T < 403 K).

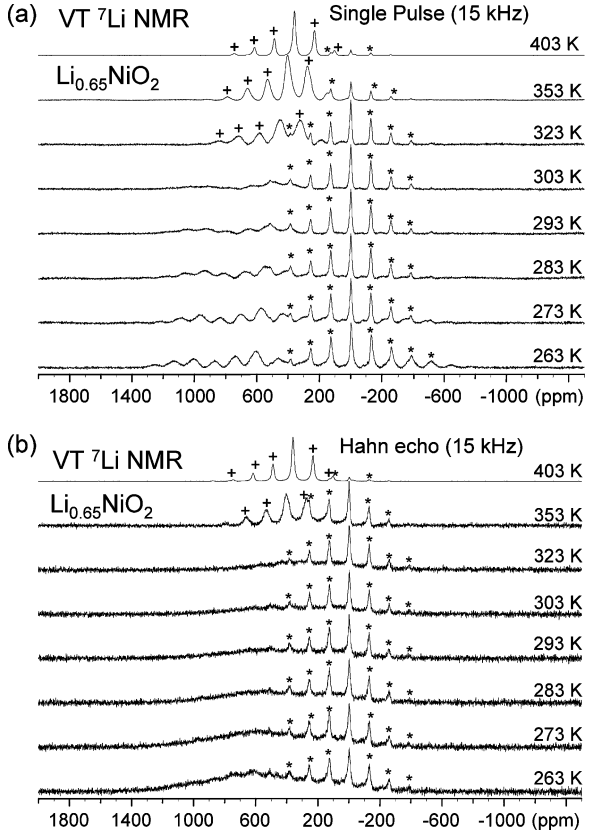

Figure 8. (a) Single-pulse and (b) synchronized-echo ^{7}Li MAS VT NMR spectra of $Li_{0.65}NiO_2$ (116.7 MHz, 15 kHz spinning, arbitrary intensities, (* and +) spinning sidebands, 263 K < T < 403 K).

$Li_{0.50}NiO_2$. The RT shift is again much higher than for a full-exchange situation and not very far from that expected from the Li/vacancy pattern found for $x = 1/2$ ($6Ni^{3+}$ with 180° and 2 Ni^{3+} with 90° configurations). The experimental and calculated shifts are indeed rather compatible if we consider that there are some differences in actual local geometry between the $Li_{0.50}NiO_2$ phase and the $LiNi_{0.30}Co_{0.70}O_2$ case from which the calculated shift was estimated. VT NMR experiments (not shown here) also showed that the signal is already exchanged at room temperature and that the beginning of the transformation of $Li_{0.50}NiO_2$ into the spinel phase occurred within the rotor at 393 K. This latter phenomenon will be addressed in a forthcoming paper.

$Li_{0.58}NiO_2$. Two different types of Li ions with different numbers of neighboring Ni^{3+} ions are expected from the ordering pattern for the closest $Li_{0.60}NiO_2$ phase. Only one signal is observed, again with a shift much higher than that corresponding to a full exchange; a single signal is[29] however consistent with an ionic-exchanged situation, but the shift is significantly higher than that corresponding to ionic hopping between the two expected Li^+ positions (i.e., the barycenter of the two expected signals, 316 ppm). Figure 7 shows the single-pulse and synchronized-echo ^{7}Li MAS NMR spectra of the $Li_{0.55}NiO_2$ phase recorded at variable temperature (295 K < T < 403 K) using a 15 kHz spinning speed, also showing that this signal is already exchanged at room temperature and remains the same with a very fast exchange rate at 403 K.

$Li_{0.65}NiO_2$. No clear pattern is obvious following Arroyo y de Dompablo's criteria. The RT signal is not really well defined, even in single-pulse conditions; its shift is however lower than that for the other x values, although there are more Ni^{3+} ions present. It is closer to, although still significantly higher than, the full-exchange one. Figure 8 shows the single-pulse and synchronized-echo ^{7}Li MAS NMR spectra of the $Li_{0.65}NiO_2$ phase recorded at variable temperature (263 K < T < 403 K) using a 15 kHz spinning speed. The signal becomes very well defined upon heating, and this is also observed in echo condition showing a very fast exchange. When the sample is returned to room temperature, the signal is identical to the one before heating (not shown), and when it is cooled to 263 K, it seems that different signals appear, which suggests that the movement becomes slow enough to observe different kinds of Li. Unfortunately, the magnetic susceptibility increases at low temperature, and the slowing down of motion restores the dipolar interaction so that the number and the width of the spinning sidebands increase and the resolution decreases drastically.

General Discussion and Conclusion

In the Li_xNiO_2 materials ($x = 0.25$, 0.33, 0.50, 0.58, and 0.65) investigated, the RT ^{7}Li NMR signals result from an

(28) Guilmard, M.; Croguennec, L.; Denux, D.; Delmas, C. *Chem. Mater.* **2003**, *15*, 4476.
(29) Wang, X.; Yang, X.; Zheng, H. H. G.; Jin, H. Y.; Zhang, Z. *J. Cryst. Growth* **2005**, *274*, 214.

exchange, and their shifts are all much higher than that corresponding to Ni^{3+}/Ni^{4+} hopping around the Li site. We therefore first conclude that the observed mobility results from ionic hopping and that no faster electronic hopping occurs independently. This is consistent with the electronic conductivity results for $x = 0.5$ considering that the hopping frequency may be small with a large number of charge carriers. The high NMR shifts observed therefore suggest that Li remains surrounded by a given number of Ni^{3+} ions at any time (i.e., that the electrons on Ni follow the Li ions in their hopping process).

For the $x = 0.25$ and 0.50 compositions, the observed shifts are not drastically different from those estimated on the basis of the Li/vacancy and Ni^{3+}/Ni^{4+} ordering patterns calculated by Arroyo y de Dompablo, if we consider that the calculated shifts are based on the known shifts due to Ni^{3+} in the $LiNi_{0.30}Co_{0.70}O_2$ material, which are likely to be altered in the Li_xNiO_2 compounds by the actual distances and angles, even though it is rather difficult to determine the local Li−O−Ni geometry experimentally.[20]

On the the other hand, for the $x = 0.33$ composition, the RT Li NMR shift is not compatible with the ordering schemes calculated by Arroyo y de Dompablo. This does not question the Li/vacancy ordering pattern since the latter was shown experimentally for $x = 0.33$ in our lab using selected area electron diffraction,[15] but this is not compatible with the proposed Ni^{3+}/Ni^{4+} pattern versus the Li/vacancy one: Li clearly appears to be surrounded by more Ni^{3+} ions with a 180° configuration.

For $x = 0.58$, the shift is also significantly higher than the barycenter of the values for the two types of Li present following Arroyo y de Dompablo's ordering patterns for $x = 3/5$, again suggesting a higher number of Ni^{3+} ions in the 180° configuration versus Li, as for the other values of x. The question of whether this is possible in an extended coupled Li/vacancy and Ni^{3+}/Ni^{4+} ordering scheme (note that experimental evidence for Li/vacancy ordering was never reported to our knowledge for $x = 3/5$ and that for $x = 0.63$ Perez et al. reported a Li/vacancy ordering pattern corresponding to the $x = 2/3$ composition from SAED data) arises.

The global situation in Li_xNiO_2 is different from that observed in the parent $Li_xNi_{0.30}Co_{0.70}O_2$ system, where, as mentioned in the Introduction, both (i.e., independent) ion and electron hopping were shown by VT NMR.[3] In the latter system, no Li/vacancy ordering has been shown, and the (random) Ni/Co distribution probably prevents the formation of a Ni^{3+}/Ni^{4+} pattern around each Li ion by hindering Jahn−Teller distortions.

Acknowledgment. The authors wish to thank B. Delatouche for technical assistance, D. Carlier and G. Ceder for extensive discussions on the ordering patterns, and Région Aquitaine (CPER Véhicule Electrique 21-13) for financial support of the NMR equipment.

IC051593N